LAMBDA-DOUBLING SPECIFICITY IN THE LOW-TEMPERATURE CAPTURE OF NO($X^2\Pi_{1/2}$) IN LOW ROTATIONAL STATES BY C^+ IONS

M. Auzinsh[a], E. I. Dashevskaya[b,c], I. Litvin[b,c], E. E. Nikitin[b,c] and J. Troe[c,d]

[a] *Department of Physics, University of Latvia, Riga LV-1586, Latvia*

[b] *Schulich Faculty of Chemistry, Technion – Israel Institute of Technology Haifa, 32000, Israel*

[c] *Max-Planck-Institut für Biophysikalische Chemie, Am Fassberg 11, Göttingen D-37077, Germany*

[d] *Institut für Physikalische Chemie, Universität Göttingen, Tammannstrasse 6, Göttingen D-37077, Germany*

Abstract

Following our general approach to Λ-doubling specificity in the capture of dipolar molecules by ions (M. Auzinsh, E. I. Dashevskaya, I. Litvin, E. E. Nikitin and J. Troe, J. Chem. Phys. **128**, 184304 (2008)), we calculate rate coefficients for the title process in the temperature range $10^{-3} < T < 10^2$ K. Three regimes are considered: i) nonadiabatic capture in a regime corresponding to a linear Stark effect of NO in the field of the incoming ion with respect to the Λ-doubling components ($10^{-1} < T < 10^2$ K), ii) adiabatic capture in the regime of an intermediate Stark effect ($10^{-3} < T < 10^{-1}$ K), iii) adiabatic capture in the limit of very low temperatures ($T << 10^{-3}$ K) in the regime of a quadratic Stark effect with respect to the Λ-doubling and hyperfine components. The results predict a high specificity of the capture rates with respect to the Λ-doubling states even under conditions when the collision energy of the partners strongly exceeds the Λ-doubling splitting.

1. Introduction

There is a growing interest in the dynamic properties of elementary chemical reaction at ultralow temperatures. On the one hand, temperatures in the range 10-20 K are relevant for interstellar molecular clouds, i.e. for astrochemical applications.[1-3] On the other hand, efficient cooling techniques for atoms and molecules [4-9] open an access to chemical reactions under sub-Kelvin laboratory conditions.

At ultralow temperatures, primarily barrierless processes are important which are initiated by capture in the long-range part of the interaction potential. Under these conditions, a variety of specific quantum effects may become apparent which would be averaged out at high temperatures. In a series of articles such as Ref. 10-14 we have investigated translational and rotational quantum effects of the reactants.

The present work considers specific low temperature quantum effects in the capture of diatomic molecules by ions, choosing the capture of $NO(X^2\Pi_{1/2})$ by C^+ ions as a representative example. It builds on previous theoretical work like Ref. 15-17, and, in particular, on Ref. 18 in which a general discussion of nonadiabatic transitions between Λ-doubling states during capture process was presented.

The rate coefficient of the capture of $NO(X^2\Pi_{1/2})$ by C^+ at low temperatures was measured in Ref. 4 at the translational temperature $T = 0.6\text{K}$. Initially, it was interpreted in the framework of a simple model that only assumed charge-permanent dipole interaction. Later it was realized that at this temperature the capture is effected also by the charge-induced dipole interaction.[15,16] The theoretical value of the capture rate coefficient, calculated for the ground rotational state of $NO(X^2\Pi_{1/2,}\, j = 1/2)$ in the adiabatic channel (AC) treatment of first-order charge-permanent dipole and charge-induced dipole interactions, was found to agree with the experimental one within experimental error.[15] Later work[17] revealed that the form of the interaction adopted in Ref. 15 and 16 for the state $j = 1/2$ provides only a poor approximation to an accurate AC potential, and that the latter is reasonably well represented by a more accurate perturbed rotor (PR) potential which includes, in addition to the first-order charge-permanent dipole and the charge-induced dipole interactions, also the second-order charge-permanent dipole interaction. This finding cast doubts on the earlier interpretation of the experiment. Indeed, it was found that the theoretical rate coefficient agrees with the experimental one only if the former is calculated for an average of

rotationally state-specific rate coefficients at a rotational temperature of about 20 K, a value also suggested in Ref. 4. It appears that state-specific rate coefficients for the capture of NO($X^2\Pi_{1/2}$,j) by C^+ such as calculated in Ref. 17 now provide enough information for the interpretation of more detailed experiments which are not necessarily related to thermal translational and rotational ensembles. One of the possible experiments could be the measurement of a capture rate, or an exothermic charge transfer event, with the participation of NO($X^2\Pi_{1/2}$) molecule in a specific rotational and Λ-doubling state. The feasibility of such an experiment is evident from recent studies of the inelastic scattering of NO and OH in selected Λ-doubling components of the ground rotational state on noble gases.[6-9]

In line with the general approach presented in Ref. 18, the aim of the present work is the calculation of Λ-doubling state-specific capture rate coefficients for NO($X^2\Pi_{1/2}$, j,ε=±1) + C^+. Low-energy (temperature) collisions for $j = 1/2$, $j = 3/2$ and $j = 5/2$ are considered and hyperfine (HF) structure effects are as well discussed for very low energies (temperatures). Section 2 describes some general features of the capture dynamics of the title process. In Section 3, the nonadiabatic (with respect to Λ-doubling states) capture of NO in the electrical field of the C^+ ion, in a regime corresponding to linear Stark effect, for $j = 1/2$, $j = 3/2$ and $j = 5/2$ states is discussed. Section 4 is devoted to adiabatic capture in a regime corresponding to intermediate Stark effect. Section 5 presents a qualitative discussion of the influence of hyperfine interaction in the ground state of NO with $j = 1/2, \varepsilon = +1$ (corresponding to a regime of quadratic Stark effect). Section 6 concludes the article.

2. Qualitative aspects of the interaction betweem NO($X^2\Pi_{1/2}$) in low rotational states and an ion.

The states of a free, rigid NO molecule in the electronic state $X^2\Pi_{1/2}$ within Hund's coupling case *a,* that belong to the manifold specified by the intrinsic angular momentum quantum number j, are two Λ-doubling components characterized by different molecular parity index $\varepsilon = \pm 1$ (or the parity $p = \varepsilon(-1)^{j-1/2}$) and the hyperfine (HF) states characterized by the total angular momentum quantum number F and the nuclear spin quantum number I=1. The energy levels of the free rotor $E_j = Bj(j+1)$

then are split into several components with the Λ-doubling and HF energy increments $\Delta E^{\Lambda}_{j,\varepsilon}$ and $\Delta E^{HF}_{j,\varepsilon,I,F}$, see e.g. Ref. 19:

$$
\begin{aligned}
E_j &= B_{\text{eff}} j(j+1) - D_e j^2 (j+1)^2 \\
\Delta E^{\Lambda}_{j,\varepsilon} &= -\varepsilon \frac{\rho}{2} (j+1/2) \\
\Delta E^{\text{HF}}_{j,\varepsilon,I,F}\Big|_{I=1} &= \frac{K_{1/2} - \varepsilon d (j+1/2)}{2j(j+1)} \left[F(F+1) - 2 - j(j+1) \right]
\end{aligned}
\qquad (1)
$$

Eq.(1) contains the five molecular parameters, $B_{\text{eff}}, D_e, \rho, K_{1/2}, d$ which are listed in Table 1.

The interaction of the NO molecule with an ion at large distances, which determines the capture at low energies, is composed of charge-permanent dipole, charge-permanent quadrupole and charge-induced dipole terms. As discussed in Ref. 17, a simplified representation of this interaction contains three parameters, the permanent dipole and quadrupole moments, μ_D and Q, and the isotropic polarizability α, such as also listed in Table 1, and is formulated as

$$
V(R,\gamma) = \frac{q\mu_D}{R^2} P_1(\cos\gamma) + \frac{qQ}{R^3} P_2(\cos\gamma) - \frac{q^2\alpha}{2R^4} \qquad (2)
$$

The interaction potential of Eq.(2) generates a set of adiabatic channel (AC) potentials $V_{j,m}(R)$, or their perturbed rotor (PR) counterparts $V^{\text{PR}}_{j,m}(R)$. The latter are constructed in such a way that they include the terms with the same powers of *R* as in Eq.(2), i.e. they incorporate first-order charge-permanent dipole interaction (cd), first-order charge-permanent quadrupole interaction (cq) and the Langevin (L) interaction (the sum of the charge-induced dipole interaction, cid, and the second-order charge-permanent dipole interaction).

We consider the following hierarchy of approximations for the AC potentials, which will be used in different temperature ranges. If Λ-doubling effect and hyperfine interaction are ignored, the AC potentials (or their PR counterparts) are written as $V_{j,m}(R)$ (or $V^{\text{PR}}_{j,m}(R)$). The calculation of these quantities is described in Ref. 17. If the

Λ-doubling effect is taken into account but the HF interaction is ignored, the AC potentials (or their PR counterparts) are written as $\widetilde{V}_{j,m}(R)$ (or $\widetilde{V}^{\mathrm{PR}}_{j,m}(R)$). As explained in Ref. 18, the quantities $\widetilde{V}_{j,m}(R)$ (and $\widetilde{V}^{\mathrm{PR}}_{j,m}(R)$) can be recovered from $V_{j,m}(R)$ (and $V^{\mathrm{PR}}_{j,m}(R)$) by a simple procedure. For instance, an expression for $\widetilde{V}_{j,m}(R)$ reads

$$\widetilde{V}_{j,m} = \frac{V_{j,m} + V_{j,-m}}{2} - \frac{s_m}{2}\sqrt{\left(V_{j,m} - V_{j,-m}\right)^2 + \left(\Delta E_j^{\Lambda}\right)^2} + \frac{s_m}{2}\Delta E_j^{\Lambda} \qquad (3)$$

where ΔE_j^{Λ} is from Eq.(1) and $s_m = \mathrm{sign}(m)$. Note that the dependence of the $\widetilde{V}_{j,m}(R)$ on the sign of m enters only through s_m. The potentials $V_{j,m}(R)$ (or $\widetilde{V}_{j,m}(R)$) are formulated relative to the asymptotic energy levels of the free rotor with quantum number j (or j,ε). In the latter case, the asymptotic quantum number ε (the parity index) is related to the AC quantum number m through $\varepsilon = s_m$. We note in passing that the PR counterpart of Eq.(3), in the language of the charge-permanent dipole interaction, corresponds to the quadratic Stark effect of NO in the field of C^+ with respect to the coupling between different rotational states (also called the weak-field approximation). This, however, does not preclude the appearance of an intermediate Stark effect with respect to the coupling between different Λ-doubling components of the same j-state (as expressed by the square root in Eq.(3)), see Section 4. Limiting forms of this intermediate Stark effect, which are also discussed in this paper, are the linear (Section 3) and quadratic (Section 5) Stark effects (with respect to the coupling between different Λ-doubling components of the same j-state).

If both the Λ-doubling effect and HF interaction are taken into account, the respective AC potentials $\widetilde{\widetilde{V}}_{j,\varepsilon,F,M}$ are obtained by diagonalization of the matrix $\widetilde{\widetilde{\mathbf{V}}}$ that consists of the sum of the matrix $\mathbf{V}$ corresponding to Eq.(2) and the matrix of the Λ-doubling and HF interactions. The latter matrix is diagonal in the j,ε,F,M representation with the elements given by Eq.(1).

The potentials $\widetilde{V}_{j,m}(R)$ and $\widetilde{V}^{\mathrm{PR}}_{j,m}(R)$ were shown in Figs. 1–3 of Ref. 18. The inspection of these figures indicates a qualitatively different pattern of the AC and PR potentials that is due to the ever-increasing role of the charge-quadrupole interaction in

comparison to the decrease of the first-order charge-permanent dipole interaction, see Fig. 1 of the present article. The following remarks about the applicability of the PR approximation to the calculation of low-temperature rate coefficients for the capture of NO($X^2\Pi_{1/2}, j,\varepsilon$) by C^+, therefore, should be noted:

i) For the state $j = 1/2$, the PR approximation is applicable for $T < 0.5$ K only when the passage over the potential barrier for the AC state $j = 1/2, m = -1/2$ can be ignored. Adiabatic capture then is possible from the lower Λ-component only.

ii) For the state $j = 3/2$, the PR approximation is applicable for $T < 0.5$ K only if the AC channel $j = 3/2, m = -1/2$ can be considered as closed (though it does not look like a closed channel in the region of applicability of the PR approximation). Adiabatic capture is possible from the lower Λ-component only, when one ignores the incorrect behavior of the PR AC potential for $j = 3/2, m = -1/2$ in the indicated energy range.

iii) For the state $j = 5/2$, the PR approximation can be used only below 0.1 K when the incorrect behavior of the PR AC potentials does not affect the capture. A novel feature here is the appearance of the attractive AC potential for the $j = 5/2, m = -1/2$ state.

The above properties of the AC potentials and their PR counterparts are discussed in detail in the following sections.

3. Nonadiabatic capture of NO($X^2\Pi_{1/2}j,\varepsilon$) by C^+ at $T >> T_j^\Lambda$ in a regime corresponding to a linear Stark effect

We first consider capture at temperatures T that noticeably exceed the characteristic temperatures $T_j^\Lambda = \Delta E_j^\Lambda / k_B$ of the Λ-doubling splitting. In this range, the passage of the collision partners over the potential barriers occurs under conditions where the effective AC potentials between the molecule and the ion correspond to linear Stark effect. However, during their mutual approach to the barriers, the partners pass through a region where the quadratic Stark effect at large separations changes into linear Stark effect at the barriers. Nonadiabatic transitions between the AC potentials $\widetilde{V}_{j,m}^{PR}$ and $\widetilde{V}_{j,-m}^{PR}$ are possible in this region, and the nonadiabatic transition probability $P_{j,m}$ should be found from the solution of two coupled equations containing the amplitudes of the

$|j,m\rangle^{\mathrm{AC}}$ and $|j,-m\rangle^{\mathrm{AC}}$ states. Under the condition when the Λ-doubling spacing ΔE_j is much smaller than the collision energy E, these equations can be formulated in the "impact parameter approximation" (i.e. in the common trajectory approximation for a rectilinear trajectory with a fixed velocity v) of relative motion.[18] The important feature of this approximation is that the probability $P_{j,m}(E)$ depends on a single parameter only, the Massey parameter, and, as a consequence, it can be recovered from the probability $P_{1/2,1/2}(E)$ by the scaling:

$$P_{j,m}(E) = P_{1/2,1/2}\left(E\frac{4j(j+1)}{3|m|(2j+1)}\right) \qquad (4)$$

The energy dependence of $P_{j,m}(E)$, for j,m states with $j = 1/2, 3/2, 5/2$, is shown in Fig. 2 (only positive m are shown for the pairs $m,-m$). In order to demonstrate the validity of the common trajectory approximation, Fig. 2 also shows the values of ΔE_j^{Λ} on the energy axis. The hatched regions, for the states indicated, correspond to the passage from the adiabatic regime (to the left of the regions) to the sudden regime (to the right of the regions) with respect to the transition between the Λ-doubling states. The inspection of Fig. 2 shows that, for the states under discussion, nonadiabatic capture occurs within a temperature range between tenths and tens K, and the common trajectory approximation introduced in Ref. 18 is adequate for the calculation of nonadiabatic transition probabilities (this approximation breaks down only when the capture is essentially adiabatic, and the transition probability is negligibly small and, therefore, can be neglected).

Reduced Λ-doubling specific rate coefficients, $\tilde{\chi}_{j,\varepsilon}$, for $j = 1/2, 3/2, 5/2$ are calculated following the procedure described in Ref. 18. As before, we express the capture rate coefficients k_{capt} in reduced form $\chi = k_{\mathrm{capt}}/k_{\mathrm{L}}$ relative to the Langevin rate coefficient $k_{\mathrm{L}} = 2\pi q\sqrt{\alpha/\mu}$. Explicitly, the $\tilde{\chi}_{j,\varepsilon}$ are represented as a sum of partial rate coefficients $\tilde{\chi}_{j,m}$:

$$\widetilde{\chi}_{j,\varepsilon} = \sum_{m} \widetilde{\chi}_{j,m} \tag{5}$$

where the allowed values of m at the r.h.s. are determined by the parity index ε from the adiabatic correlation $\varepsilon = \mathrm{sign}(m)$, implying that m are positive for the lower Λ-doubling component with $\varepsilon = +1$ and negative for the upper one with $\varepsilon = -1$. In turn, the $\widetilde{\chi}_{j,m}$ are expressed through survival (surv) and transition (trans) rate coefficients $\chi_{j,m}^{\mathrm{surv/trans}}$ which are calculated using the probabilities $P_{j,m}^{\mathrm{surv/trans}}$ (which account for the Λ-doubling effect) and the effective AC potentials $U_{j,m}(R,J)$ (that ignore the Λ-doubling effect). The above is concisely expressed through the following set of equations (see Ref. 18 for details)

$$\widetilde{\chi}_{j,m} = 2\chi_{j,m}^{\mathrm{surv}} + 2\chi_{j,-m}^{\mathrm{trans}} \tag{6}$$

$$\chi_{j,m}^{\mathrm{surv/trans}} = A(T) \int_{0}^{\infty} \frac{JdJ}{2j+1} \int_{U_{j,m}^{\max}(J)}^{\infty} P_{j,m}^{\mathrm{surv/trans}}(E) \exp\left(-E/k_{\mathrm{B}}T\right) \frac{dE}{k_{\mathrm{B}}T} \tag{7}$$

$$A(T) = \sqrt{\frac{8k_{\mathrm{B}}T}{\pi\mu}} \frac{\pi\hbar^2}{\mu k_{\mathrm{B}}T} \frac{1}{2\pi q} \sqrt{\frac{\mu}{\alpha}} \tag{8}$$

$$P_{j,m}^{\mathrm{surv}}(E) = 1 - P_{j,m}(E) \qquad \text{and} \qquad P_{j,m}^{\mathrm{trans}}(E) = P_{j,m}(E) \tag{9}$$

The energy $U_{j,m}^{\max}(J)$ entering in Eq.(7) is defined through the properties of the effective AC potentials, composed of the AC potential and the classical centrifugal energy

$$U_{j,m}(R,J) = \frac{\hbar^2 (J+1/2)^2}{2\mu R^2} + V_{j,m}(R) \tag{10}$$

Explicitly, $U_{j,m}^{\max}(J)$ in Eq.(7) corresponds to the maximum of the effective potential $U_{j,m}(R,J)$ from Eq.(10) if the latter possesses a barrier; it is equal to zero, if $U_{j,m}(R,J)$ is attractive, and it is infinity, if $U_{j,m}(R,J)$ is repulsive.

In particular, for the states with $j=1/2$ there exists a one-to-one correspondence between ε and m, $\varepsilon = 2m$, such that the expression for $\widetilde{\chi}_{1/2,\varepsilon}$ assumes the form

$$\widetilde{\chi}_{1/2,\varepsilon} = A(T)\int_0^\infty JdJ\left\{\int_{U_{1/2,\varepsilon/2}^{\mathrm{AC,max}}(J)}^{\infty}\left(1-P_{1/2,1/2}(E)\right)\exp\left(-E/k_{\mathrm{B}}T\right)\frac{dE}{k_{\mathrm{B}}T}+\right.$$
$$\left.+\int_{U_{1/2,-\varepsilon/2}^{\mathrm{AC,max}}(J)}^{\infty}\left(P_{1/2,1/2}(E)\right)\exp\left(-E/k_{\mathrm{B}}T\right)\frac{dE}{k_{\mathrm{B}}T}\right\} \qquad (11)$$

The results of accurate calculations of $\widetilde{\chi}_{1/2,\varepsilon}$ are presented in Fig. 3, along with the effective rate coefficient $\widetilde{\chi}_{1/2}^{\mathrm{eff}}$ for the capture from thermally populated Λ-components, and the capture rate coefficient $\chi_{1/2}^{\mathrm{AC}}$ calculated earlier neglecting Λ-doubling effects.[17] These are expressed as

$$\widetilde{\chi}_{1/2}^{\mathrm{eff}} = \frac{\widetilde{\chi}_{1/2,+}+\widetilde{\chi}_{1/2,-}\exp\left(-\Delta E_{1/2}^{\Lambda}/k_{\mathrm{B}}T\right)}{1+\exp\left(-\Delta E_{1/2}^{\Lambda}/k_{\mathrm{B}}T\right)} \qquad (12)$$
$$\chi_{1/2}^{\mathrm{AC}} = \left(\widetilde{\chi}_{1/2,+}+\widetilde{\chi}_{1/2,-}\right)/2$$

As noted in Ref. 17, the accurate rate coefficients below 10 K are well approximated by their PR counterparts calculated with PR AC potentials given by

$$V_{1/2,m}^{\mathrm{PR}}(R) = -m\frac{2\mu_D q}{3R^2}-\frac{q^2\alpha^{PR}}{2R^4} \qquad (13)$$

When this expression for the potentials is complemented by the approximate analytical expression for $P(E)_{1/2,1/2}$,

$$P_{1/2,1/2}(E) = \frac{\exp\left(-(c/2)\tilde{J}_{1/2,1/2}\sqrt{\Delta E^{\Lambda}_{1/2}/E}\right)}{1+\exp\left(-(c/2)\tilde{J}_{1/2,1/2}\sqrt{\Delta E^{\Lambda}_{1/2}/E}\right)} \tag{14}$$

with the numerical coefficient $c = 2.396$ and $\tilde{J}_{1/2,1/2} = \left(2\mu\mu_{\mathrm{D}}q/3\hbar^2\right)^{1/2} = 25.62$ from Ref. 18, the calculation of $\tilde{\chi}^{\mathrm{PR}}_{1/2,\varepsilon}$ becomes quite easy. In particular, as follows from Fig. 2, the capture below 1 K occurs adiabatically with respect to the Λ-doubling states and, therefore, $\tilde{\chi}_{1/2,\varepsilon} = \tilde{\chi}^{\mathrm{adia}}_{1/2,\varepsilon}$ can be expressed through the partial rate coefficients $\chi_{1/2,m}$ in which Λ-doubling is ignored. Since the latter are well approximated by their PR counterparts and represented analytically,[18] for instance, over the range $T^{\Lambda}_{1/2} << T < 0.1$ K we obtain the following expression for $\tilde{\chi}^{\mathrm{adia}}_{1/2,+}$,

$$\tilde{\chi}^{\mathrm{adia}}_{1/2,+}(T) \approx \chi^{\mathrm{PR}}_{1/2,+}(T) = 2\chi^{\mathrm{PR}}_{1/2,1/2} = 2\sqrt{\frac{\alpha^{\mathrm{PR}}}{\alpha}}\left[\frac{1}{6}\sqrt{\frac{2\mu_D^2}{\pi\alpha^{\mathrm{PR}}k_{\mathrm{B}}T}}+\frac{1}{2}\right] \tag{15}$$

Towards the high-temperature side of the graphs in Fig.3, the quantities $\tilde{\chi}^{\mathrm{eff}}_{1/2}$ and $\chi^{\mathrm{PR}}_{1/2}$ level off at a temperature of about 10 K which indicates that the capture mainly occurs when the attractive potential is proportional to R^{-4}. This potential differs from the ion-induced dipole potential $-q^2\alpha/2R^4$ because it also contains second-order corrections from the charge-permanent dipole interaction. The leveling-off then occurs at values which are higher than the true high-temperature limit of unity. At the low-temperature side, $\tilde{\chi}^{\mathrm{eff}}_{1/2}$ and $\chi^{\mathrm{AC}}_{1/2}$ slightly deviate from each other due to the thermal population factor $\exp(-\Delta E^{\Lambda}_j/k_{\mathrm{B}}T)$. The small difference between $\tilde{\chi}^{\mathrm{eff}}_{1/2}$ and $\chi^{\mathrm{AC}}_{1/2}$, of course, does not imply that the capture is close to the sudden limit.

For other states ($j = 3/2, 5/2$), the PR approximation is only applicable at substantially lower temperatures, and the calculation of $\tilde{\chi}_{3/2,\varepsilon}$ and $\tilde{\chi}_{5/2,\varepsilon}$ should be based on accurate AC potentials. Figures 4 and 5 present graphs of $\tilde{\chi}_{j,\varepsilon}$ for the temperature range 0.1<*T*<100 K, such as calculated with accurate AC potentials $V_{j,m}(R)$ and accurate transition probabilities. Also shown are χ^{AC}_j and the effective rate

coefficients $\widetilde{\chi}_j^{\rm eff}$ that are defined similar to Eq.(12). Compared to j=1/2, a qualitatively new feature for j=3/2 is the passage of the rate coefficients through minima. This is due to the interplay between a weaker charge-dipole interaction and the charge-quadrupole interaction which is absent for j=1/2. An even more drastic difference is observed when one compares the cases j=3/2 and j=5/2. In the latter case, due to the relatively larger effect of the charge-quadrupole interaction, the capture from the upper Λ-component becomes possible at lower temperatures. The common important feature for all three cases is that, at temperatures below 1 K which is still much higher than the characteristic temperature for the Λ-doubling splitting, the capture from individual Λ-doubling states occurs adiabatically. This allows one to treat the capture below 1 K within the standard AC approach, using AC potentials that explicitly take into account the Λ-doubling splitting.

4. Adiabatic capture of NO($X^2\Pi_{1/2}j,\varepsilon$) by C^+ in a regime corresponding to an intermediate Stark effect

In a regime corresponding to an intermediate Stark effect, capture occurs under adiabatic conditions. It then follows that for T<0.1 K and j=1/2 and 3/2, capture occurs only from the lower Λ-component ($\varepsilon = +1$) through the AC channels $\widetilde{V}_{1/2,1/2}$ and $\widetilde{V}_{3/2,1/2}$, $\widetilde{V}_{3/2,3/2}$, respectively, while, for j=5/2, beside the capture channels with $m = 1/2, 3/2, 5/2$ correlating with $\varepsilon = +1$ state, there exists a channel with $m = -1/2$ that correlates with the upper Λ-component ($\varepsilon = -1$). For $T < 0.1\,\mathrm{K}$, one can use PR potentials $\widetilde{V}_{j,m}(R)$ which are derived from Eq.(3). The explicit form of these potential is

$$\widetilde{V}^{\rm PR}_{j,m}(R) = \widetilde{V}^{\rm cd}_{j,m}(R) + V^{\rm cq}_{j,m}(R) + V^{\rm L}_{j,m}(R) \qquad (16)$$

Here,

$$\widetilde{V}^{\rm cd}_{j,m}(R) = -\frac{\mathrm{sign}(m)}{2}\sqrt{(\Delta E^{\Lambda}_j)^2 + \frac{q^2\mu_D^2 m^2}{R^4 j^2 (j+1)^2}} + \mathrm{sign}(m)\,\Delta E_j/2, \qquad (17)$$

$$V_{j,m}^{\mathrm{cq}}(R)=\frac{qQ}{R^3}\frac{\left(j(j+1)-3m^2\right)}{(2j+3)(2j-1)}\frac{\left(j(j+1)-3/4\right)}{j(j+1)}, \tag{18}$$

$$V_{j,m}^{\mathrm{L}}(R)=-\frac{\alpha q^2}{2R^4}\left\{1-\frac{\mu_D^2}{\alpha B}\left(\frac{(j^2-1/4)(j^2-m^2)}{j^3(2j-1)(2j+1)}-\frac{\left((j+1)^2-1/4\right)\left((j+1)^2-m^2\right)}{(j+1)^3(2j+1)(2j+3)}\right)\right\} \tag{19}$$

The capture rate coefficient for the AC PR potential in the adiabatic regime then assumes the standard form. Explicitly, $\widetilde{\chi}_{j,\varepsilon}$ are represented as a sum of partial rate coefficients $\widetilde{\chi}_{j,m}$, see Eq. (5), and the latter are identified with partial adiabatic capture rate coefficients

$$\widetilde{\chi}_{j,m}^{\mathrm{PR}}=A(T)\int_0^{\infty}\frac{JdJ}{2j+1}\int_{\widetilde{U}_{j,m}^{\mathrm{PR,max}}(J)}^{\infty}\exp\left(-E/k_{\mathrm{B}}T\right)\frac{dE}{k_{\mathrm{B}}T} \tag{20}$$

Here $\widetilde{U}_{j,m}^{\mathrm{PR\,max}}(J)$ is the maximum of the effective potential

$$\widetilde{U}_{j,m}^{\mathrm{PR}}(R,J)=\frac{\hbar^2(J+1/2)^2}{2\mu R^2}+\widetilde{V}_{J,m}^{\mathrm{PR}}(R) \tag{21}$$

Again we start with the case j=1/2, since it is simplest because the first-order charge-quadrupole interaction vanishes. Then the attractive potential $\widetilde{V}_{1/2,1/2}^{\mathrm{PR}}$ collapses into its simplified version

$$\widetilde{V}_{1/2,1/2}^{\mathrm{PR}}(R)=-\frac{1}{2}\sqrt{\left(\frac{2\mu_D q}{3R^2}\right)^2+\left(\Delta E_{1/2}^{\Lambda}\right)^2}-\frac{q^2\alpha^{\mathrm{PR}}}{2R^4}+\frac{1}{2}\Delta E_{1/2}^{\Lambda} \tag{22}$$

As argued in Ref. 18, the rate coefficient for capture in the field of the potential of Eq.(22) can be related to $\chi_{1/2,+}^{\mathrm{PR}}$ through a damping function $F(T_{1/2}^{\Lambda}/T)$, i.e.

$$\tilde{\chi}^{\mathrm{PR}}_{1/2,+}(T) \approx \tilde{\chi}^{\mathrm{PR,app}}_{1/2,+}(T) = 2\,\chi^{\mathrm{PR}}_{1/2,1/2}(T) F(T^{\Lambda}_{1/2}/T) \qquad (23)$$

where $\chi^{\mathrm{PR}}_{1/2,1/2}(T)$ is defined by Eq.(15) and

$$F(x) = \int_0^1 dy \exp\left[-(x/2)(1-\sqrt{1-y^2})\right] \qquad (24)$$

The function $F(T^{\Lambda}_{1/2}/T)$ has the asymptotic behavior

$$F(x) = \begin{cases} 1, & x << 1 \\ \sqrt{\pi/x}, & x >> 1 \end{cases} \qquad (25)$$

which damps the $T^{-1/2}$ divergence of $\chi^{\mathrm{PR}}_{1/2,1/2}$ (arising from its cd contribution) and brings the $\tilde{\chi}^{\mathrm{PR,app}}_{1/2,+}$ rate to a constant limit at very low temperatures when $T << T^{\Lambda}_{1/2}$:

$$\tilde{\chi}^{\mathrm{PR,app}}_{1/2,+}(T)\Big|_{T<<T^{\Lambda}_{1/2}} = \sqrt{\tilde{\alpha}/\alpha}, \quad \tilde{\alpha} = 2(\mu_D)^2/9\Delta E^{\Lambda}_{1/2}, \qquad (26)$$

As discussed in Ref. 18, the approximate expression $\tilde{\chi}^{\mathrm{PR,app}}_{1/2,+}(T)\Big|_{T<<T^{\Lambda}_{1/2}}$ differs from the accurate one $\tilde{\chi}^{\mathrm{PR}}_{1/2,+}(T)\Big|_{T<<T^{\Lambda}_{1/2}}$ by a relative correction $\alpha^{\mathrm{PR}}/2\tilde{\alpha}$ which is small unless the dipole moment is anomalously low.

Fig. 6 shows plots of the rate coefficients $\tilde{\chi}^{\mathrm{PR}}_{1/2,+}$ as well as the approximate expressions $\tilde{\chi}^{\mathrm{PR,app}}_{1/2,+}$ and $\tilde{\chi}^{\mathrm{PR,eff}}_{1/2}$. For comparison, plots of extrapolated values of $\chi^{\mathrm{PR,}}_{1/2,1/2}$ and $\chi^{\mathrm{PR,eff}}_{1/2}$ are also shown. At the r. h. s. of this figure, the damping is negligible and the graphs coalesce to two filled circles that correspond to those at the l. h. s. of Fig. 3. At the l. h. s. of Fig. 6, both $\chi^{\mathrm{PR}}_{1/2,1/2}$ and $\chi^{\mathrm{PR,eff}}_{1/2}$ diverge as $T^{-1/2}$ while $\tilde{\chi}^{\mathrm{PR}}_{1/2,+}$ and $\tilde{\chi}^{\mathrm{PR,eff}}_{1/2}$ tend to a limit that approximately corresponds to $\sqrt{\tilde{\alpha}/\alpha}$. We note also that the approximation of Eq.(23) performs quite satisfactorily.

For higher values of *j*, the capture rate coefficients were calculated using the full AC PR potentials from Eqs.(16)–(19). The comparison of the graphs presented in Fig. 7 shows that $\widetilde{\chi}^{\mathrm{PR}}_{3/2,+}$ is noticeably lower than $\widetilde{\chi}^{\mathrm{PR}}_{1/2,+}$. This is ascribed to a much weaker charge-dipole interaction which arises from two effects: the smaller value of the dipole moment in the state *j*=3/2, and the stronger suppression of the cd interaction in the regime of the intermediate Stark effect (because of the larger value of the Λ-doubling splitting). These effects become even more pronounced for *j*=5/2. A new feature appears here, the capture from the upper component of the Λ-doublet. The nonzero value of $\widetilde{\chi}^{\mathrm{PR}}_{5/2,-}$ is the result of the competition between the attractive first-order charge-quadrupole interaction and the repulsive charge-permanent dipole interaction in the intermediate Stark effect regime. A noticeable negative temperature dependence of $\widetilde{\chi}^{\mathrm{PR}}_{5/2,-}$ signals the prevailing influence of the charge-quadrupole interaction that manifests itself in the incipient $T^{-1/6}$ divergence of the classical rate which is quenched in the quantum regime, see Section 5.

5. Adiabatic capture of NO($X^2\Pi_{1/2,j=1/2}$) by C^+ in a regime corresponding to a quadratic Stark effect. The effect of the HF interaction.

The calculation of the capture rate coefficients in the previous sections ignored the HF structure. However, when the capture occurs at ultra low temperatures, the calculation of the rate coefficients should be based on PR AC potentials that include both the Λ-doubling and the HF interaction. These potentials, $\widetilde{\widetilde{V}}_{j,\varepsilon,F,M}$, can be found by numerical diagonalization of a matrix with diagonal elements $\Delta E^{\Lambda}_{j,\varepsilon} + \Delta E^{HF}_{j,\varepsilon,I,F}$ and off-diagonal elements derived from the matrix $V^{\mathrm{PR}}_{j,m}(R)$ by transforming it from the j,m,I,M_I representation to the j,I,F,M representation[20] where $I=1$ is the total nuclear spin (that coincides with the nuclear spin of the nitrogen), M_I is its projection onto the collision axis, F is the total angular momentum of NO ($\mathbf{F}=\mathbf{j}+\mathbf{I}$) and M is its projection onto the collision axis. We illustrate the general pattern of AC potentials for the case $j=1/2$ since in this case the HF structure is rather simple (due to the condition $j<I=1$, F assumes only two values, 1/2 and 3/2) and the charge-quadrupole

interaction vanishes. We also replace the matrix $\mathbf{V}^{\mathrm{PR}}$ by $\mathbf{V}^{\mathrm{cd}}$ since the charge-dipole interaction makes the largest contribution and we drop the subscripts j and I which are the same ($j=1/2, I=1$) in all equations below.

Figures 8 and 9 show plots of the scaled CD AC potentials $\upsilon_{\varepsilon,F,M}=\tilde{\tilde{V}}_{\varepsilon,F,M}\big/\Delta E^{\Lambda}_{1/2}$ vs. the scaled CD interaction energy $\eta=q\mu_D\big/\Delta E^{\Lambda}_{1/2}R^2$ in two regions. Fig. 8 covers the range from free fragments ($\eta=0$) to the middle of the intermediate Stark effect region for Λ-doubling states ($\eta=6$). Interesting features of Fig. 8 are the comparison of the accurate AC potentials $\upsilon_{\varepsilon,F,M}$ with their low-energy counterpart (the second order Stark effect for HF states) at the weak-interaction side ($\eta<1$), and the behavior of the potentials $\upsilon_{\varepsilon,F,M}$ at the medium-interaction side ($\eta\approx 4$) (full lines). At the weak interaction side, the AC cd potentials are given by general expressions from second-order perturbation theory[21] with respect to Λ-doubling and HF spacing, yielding a Langevin-type interaction of the form

$$\tilde{\tilde{V}}^{\text{cd-L}}_{j,\varepsilon,I,F,M}(R)=-\frac{q^2\tilde{\tilde{\alpha}}_{j,\varepsilon,I,F,M}}{2R^4} \tag{27}$$

$$\begin{aligned}
&\tilde{\tilde{\alpha}}_{j,\varepsilon,I,F,M}=\tilde{\alpha}G_{j,\varepsilon,I,F,M}= \\
&=\tilde{\alpha}\left\{\frac{\Delta E^{\Lambda}_{1/2}M^2\left[j(j+1)+F(F+1)-I(I+1)\right]^2}{\left(E_{j,\mp\varepsilon,I,F}-E_{j,\pm\varepsilon,I,F}\right)F^2(F+1)^2}+\right. \\
&+\frac{\Delta E^{\Lambda}_{1/2}\left(F^2-M^2\right)\left(F+j+I+1\right)\left(j-F+I+1\right)\left(F-j+I\right)\left(j+F-I\right)}{\left(E_{j,\mp\varepsilon,I,F-1}-E_{j,\pm\varepsilon,I,F}\right)F^2(2F+1)(2F-1)}+ \\
&\left.+\frac{\Delta E^{\Lambda}_{1/2}\left((F+1)^2-M^2\right)\left(F+j+I+2\right)\left(j-F+I\right)\left(F-j+I+1\right)\left(j+F+1-I\right)}{\left(E_{j,\mp\varepsilon,I,F+1}-E_{j,\pm\varepsilon,I,F}\right)(F+1)^2(2F+3)(2F+1)}\right\}
\end{aligned} \tag{28}$$

where one should put $j=1/2, I=1$. If all energy differences in the denominators of Eq.(28) are equal to $\Delta E^{\Lambda}_{1/2}$, one finds that all G coefficients are equal to either 1 or –1, i.e. we return to the case of vanishing HF interaction (dotted lines in Fig. 8). On the other hand, if one substitutes the energy differences according to Eq.(1) with $j=1/2, \varepsilon=+1, I=1$, for $G_{F,M}\equiv G_{j,\varepsilon,I,F,M}\big|_{j=1/2,\varepsilon=+1,I=1}$ the following values are

obtained: $G_{1/2,1/2} = 1.545$, $G_{3/2,1/2} = 1.762$, $G_{3/2,3/2} = 0.703$ (note that the G are positive for attractive states). The AC cd energies in second order are shown in Fig. 8 by dashed curves. In the medium interaction region, where the approach to the linear Stark effect is already noticeable, the full curves run more or less parallel to the dotted ones. The rather simple pattern of the AC potentials is the consequence of a vanishing coupling, in the electrical field of the ion, between different F-states belonging to the same parity.

Fig. 9 shows the energies from regimes of the intermediate to the linear Stark effect. The potentials $\upsilon_{\varepsilon,F,M}$ here are shown on a logarithmic scale (full lines) in order to demonstrate the convergence to their cd counterpart when the HF coupling is neglected (dashed lines). The disappearance of the HF interaction with increasing η in this figure is actually an artifact of the logarithmic representation, since part of the HF interaction survives as a first-order correction to the AC potentials V_m^{cd}. Nonetheless, this disappearance supports the conclusion that the capture at large energies can be treated neglecting the small HF corrections to the interaction potential. Supplemented with the effective Langevin interaction, the AC potentials in Figures 8 and 9 provide the necessary information for calculating the accurate capture rate coefficients over a very wide temperature range with accounting both for the Λ-doubling and HF effects.

Using the AC cd potentials, in the following we consider the low-temperature asymptotes of the partial rate coefficient $\widetilde{\widetilde{\chi}}^{\mathrm{cd\text{-}L}}_{F,M}$ in the regime corresponding to second-order Stark effect (we use $\widetilde{\widetilde{\chi}}^{\mathrm{cd\text{-}L}}_{F,M}$ as a shortened notation for $\left.\widetilde{\widetilde{\chi}}^{\mathrm{cd-L}}_{j,\varepsilon,I,F,M}\right|_{j=1/2,\varepsilon=+,I=1}$). After some simple manipulations and with the use of the asymptotic rate coefficients, from Eq.(27) we obtain:

$$\begin{aligned}
\widetilde{\widetilde{\chi}}^{\mathrm{cd\text{-}L}}_{1/2,1/2} &= \sqrt{\widetilde{\alpha}/\alpha}\sqrt{G_{1/2,1/2}} = 1.243\sqrt{\widetilde{\alpha}/\alpha} \\
\widetilde{\widetilde{\chi}}^{\mathrm{cd\text{-}L}}_{3/2,1/2} &= \sqrt{\widetilde{\alpha}/\alpha}\sqrt{G_{3/2,1/2}} = 1.327\sqrt{\widetilde{\alpha}/\alpha} \\
\widetilde{\widetilde{\chi}}^{\mathrm{cd\text{-}L}}_{3/2,3/2} &= \sqrt{\widetilde{\alpha}/\alpha}\sqrt{G_{3/2,3/2}} = 0.838\sqrt{\widetilde{\alpha}/\alpha}
\end{aligned} \qquad (29)$$

The effective rate coefficient $\widetilde{\widetilde{\chi}}^{\text{cd-L,eff}}$, for equal populations of two HF levels $F = 3/2$ and $F = 1/2$, amounts to $1.136\sqrt{\widetilde{\alpha}/\alpha}$, and it drops to $1.083\sqrt{\widetilde{\alpha}/\alpha}$ for the case of prevailing population of the lower HF state with $F = 3/2$. The value of the latter is marked by an arrow at the left hand side of Fig. 6.

The extrapolation of the expressions in Eq.(29) to zero temperature requires a generalization of the AC approach in two respects: for ultra-low temperatures of the order of $T_{\text{ULT}} = \hbar^4 / k_{\text{B}} q^2 \widetilde{\alpha} \mu^2$ and below, one has to take into account the quantum character of relative motion (quantization of the total angular momentum, tunneling through and reflection above centrifugal barriers)[10] and the Coriolis coupling between AC states with different values of *M*, see Ref. 11 The latter is satisfactorily described by the axially nonadiabatic approach, which does not modify the AC result for $F = 1/2$ with a single AC potential but merges the set of two AC potentials for $F = 3/2$ into a single average potential.[11] In this way, the zero-temperature limit of the rate coefficients $\widetilde{\widetilde{\chi}}^{\text{cd-L}}_{1/2}$ and $\widetilde{\widetilde{\chi}}^{\text{cd-L}}_{3/2}$ for the states $F = 1/2$ and $F = 3/2$ respectively are given by the Vogt-Wannier[22] expressions:

$$\lim\left(\widetilde{\widetilde{\chi}}^{\text{cd-L}}_{1/2}\right)_{T\to 0} = 2\sqrt{\widetilde{\alpha}/\alpha}\sqrt{G_{1/2,1/2}} = 2.486\sqrt{\widetilde{\alpha}/\alpha}$$

$$\lim\left(\widetilde{\widetilde{\chi}}^{\text{cd-L}}_{3/2}\right)_{T\to 0} = 2\sqrt{\widetilde{\alpha}/\alpha}\sqrt{\left(G_{3/2,1/2} + G_{3/2,3/2}\right)/2} = 2.220\sqrt{\widetilde{\alpha}/\alpha} \qquad (30)$$

The qualitative character of the temperature dependence of the rates within the range $T_{\text{ULT}} < T < T^{\Lambda}_{1/2}$ can be inferred by expressing T_{ULT} through the parameters of the problem under discussion. Substituting $\widetilde{\alpha}$ from Eq.(26) into the expression for T_{ULT}, we find $T_{\text{ULT}} \approx 2\Delta E^{\Lambda}_{1/2} / k_{\text{B}} \widetilde{J}^4_{1/2,1/2} = 2T^{\Lambda}_{1/2} / \widetilde{J}^4_{1/2,1/2}$. Since $\widetilde{J} >> 1$ (see Section 3), we see that the quantum regime in the capture occurs much below the characteristic temperature T^{Λ} corresponding to the Λ-doubling and, therefore, the plots of the functions $\widetilde{\widetilde{\chi}}^{\text{CD}}_{F}(T)$ will exhibit a wide plateau within the range $T_{\text{ULT}} < T < T^{\Lambda}_{1/2}$ (as given by Eq.(29)), before they turn up, at $T < T_{\text{ULT}}$, to their zero-temperature limits (as given by Eq.(30)).

6. Discussion and conclusion

The capture of NO in the lowest rotronic states $X^2\Pi_{1/2,j,\varepsilon}$, with $j = 1/2, 3/2, 5/2; \varepsilon = \pm 1$, by C^+ demonstrates several general features of low-temperature complex-formation in collisions of a dipolar molecule in a degenerate electronic state with an ion. The state-specific rate coefficients strongly depend on the Λ-doubling state even under conditions when the translational temperature T is much higher than the characteristic temperature T_j^Λ of the Λ-doubling splitting. This feature is a consequence of the very slow variation of the perturbation exerted on the molecule by the electric field of the ion upon mutual approach of the partner across a region corresponding to an intermediate Stark effect. With decreasing temperature, but for T still higher than T_j^Λ, the capture occurs adiabatically with respect to transitions between adiabatic channel potentials correlating with different Λ-doubling components. Under this condition, the capture from the upper Λ-doubling component does not occur at all for $j = 1/2$ and $j = 3/2$, but it does occur for $j = 5/2$. The qualitative difference between these two cases is due to the subtle interplay between the charge-dipole interaction in the intermediate Stark effect and charge-quadrupole interaction. This difference demonstrates what happens when the projection of the permanent dipole moment onto the intrinsic angular momentum vector **j**, as a result of the rotational averaging of the dipole moment with increase of j, becomes small. The capture rate coefficient from the lower Λ-doubling component is quenched compared to its purely charge-permanent dipole (linear Stark effect) counterpart and, in the limit of very low temperature, at $T << T_j^\Lambda$, the rate coefficient is determined by an interaction consisting of a Langevin-type term, formed by a second-order Stark effect component of the molecular dipole in the external field of the ion (proportional to R^{-4}) and a charge-quadrupole term (proportional to R^{-3}). The inclusion of the hyperfine interaction neither drastically modifies the qualitative picture of the temperature dependence of the rate coefficients nor the nonadiabatic/adiabatic capture dynamics, since the electric field of the ion does not couple hyperfine structure states belonging to the same Λ-doubling component. For the same reason, the rate coefficients at ultra-low temperatures, when the relative motion of the partners shows quantum features, and their zero-temperature limits do not deviate drastically from the rate coefficients at very low temperatures.

However, the capture dynamics under the latter condition is complicated by the fact that the Coriolis coupling tends to average the first-order charge-quadrupole interaction proportional to R^{-3} (effective for higher temperatures). As a result, the consequences of the charge-quadrupole interaction are second-order terms (with respect to the states of the relative rotation of the partners) being proportional to R^{-4}, see Ref. 12. Thus, the overall potential which is responsible for the capture in the ULT regime, behaves again like an effective Langevin interaction. On the whole, one can say that the apparent low-temperature divergence of the capture rate coefficients of a dipolar and quadrupolar molecule in an open electronic state by an ion with decreasing temperature is removed by two effects: first, the $T^{-1/2}$ divergence from the cd interaction is removed by the nonadiabatic rotronic coupling between the given and other electronic states (which results in the Λ-doubling) and, second, the $T^{-1/6}$ divergence from the cq interaction is removed by the nonadiabatic rotational coupling which manifests itself in the averaging of the first-order cq interaction to zero. As a result, the state-specific Λ-doubling and HF capture rate coefficients tend to constant values at zero temperature which correspond to an effective Langevin interaction.

Acknowledgement

Financial support of this work by EU Human Potential MCRTIN 512302 "The Molecular Universe" is gratefully acknowledged. E.N also acknowledges the support by the award from the Alexander von Humboldt Foundation.

Appendix. Glossary of abbreviations used in this paper

i) AC = Adiabatic Channel, PR = Perturbed Rotor, cd = charge-permanent dipole, L = Langevin, HF = hyperfine.

ii) $\chi_{j,m}^{\mathrm{AC}}$, χ_{j}^{AC} are reduced partial (*j,m*-specific) and total (*j*-specific) AC capture rate coefficients calculated with Λ-doubling effects ignored (i.e. corresponding to a sudden transition between the Λ-components). With AC replaced by PR, the rate coefficients $\chi_{j,m}^{\mathrm{PR}}$, χ_{j}^{PR} corresponds to AC PR potentials. With AC replaced by cd, the rate

coefficients $\chi^{\mathrm{cd}}_{j,m}$, χ^{cd}_{j} correspond to the cd interaction in a regime corresponding to a linear Stark effect.

iii) $\widetilde{\chi}_{j,m}$, $\widetilde{\chi}_{j,\varepsilon}$ are reduced partial (*j,m*-specific) and total (*j,ε*-specific) capture rate coefficients calculated accounting for nonadiabatic transitions between AC potentials.

iv) $\chi^{\mathrm{surv/trans}}_{j,m}$ are reduced auxiliary capture rate coefficients corresponding to survival on a j,m AC potential and to transition between $j,m \to j,-m$ AC potentials for the motion across the nonadiabaticity region.

v) $\widetilde{\chi}^{\mathrm{PR}}_{j,m}$, $\widetilde{\chi}^{\mathrm{PR}}_{j,\varepsilon}$ are reduced partial (*j,m*-specific) and total (*j,ε*-specific) AC PR capture rate coefficients calculated with Λ-doubling effect taken into account. With PR replaced by cd, the rate coefficients $\widetilde{\chi}^{\mathrm{cd}}_{j,m}$, $\widetilde{\chi}^{\mathrm{cd}}_{j,\varepsilon}$ correspond to the cd interaction in the intermediate Stark effect regime. With PR replaced by cd-L, the rate coefficients $\widetilde{\chi}^{\mathrm{cd\text{-}L}}_{j,m}$, $\widetilde{\chi}^{\mathrm{cd\text{-}L}}_{j,\varepsilon}$ correspond to the cd interaction in the quadratic Stark effect regime where the AC PR potentials are represented by effective Langevin-type (L) terms

vi) $\widetilde{\widetilde{\chi}}^{\mathrm{cd-L}}_{F,M} \equiv \left.\widetilde{\widetilde{\chi}}^{\mathrm{cd-L}}_{j,\varepsilon,I,F,M}\right|_{j=1/2,\varepsilon=+,I=1}$ are the reduced partial (*F,M*, *j,*ε -specific) AC cd capture rate coefficients calculated with Λ-doubling and hyperfine effects taken into account in the quadratic Stark effect regime with respect to the Λ-doubling hyperfine splitting.

References

1. E. Herbst, J. Phys. Chem. A **109**, 4017 (2005).
2. H. Sabbah, L. Biennier, I. R. Sims, Yu. Georgievskii, S. J. Klippenstein, and I. W. M. Smith, Science **317**, 102 (2007).
3. I. W. M. Smith, A. M. Sage, N. M. Donahue, E. Herbst, and D. Quan, Faraday Discuss. **133**, 137 (2006)
4. T. L. Mazely and M. A. Smith, Chem. Phys. Lett. **144**, 563 (1988).
5. S. Willitsch, M. T. Bell, A. D. Gingell, S. R. Procter, and T. P. Softley, Phys. Rev. Lett. **100**, 043203 (2008).
6. J. J. van Leuken, J. Bulthuis, S. Stolte, and J. G. Snijders, Chem. Phys. Lett. **260**, 595 (1996).
7. A. Gijsbertsen, H. Linnartz, G. Rus, A. E. Wiskerke, S. Stolte, D. W. Chandler, and J. Kłos, J. Chem. Phys. **123**, 224305 (2005).
8. S. Y. T. van de Meerakker, P. H. M. Smeets, N. Vanhaecke, R. T. Jongma, and G.Meijer, Phys. Rev. Lett. **94**, 023004 (2005).
9. J. J. Gilijamse, S. Hoekstra, S. Y. T. van de Meerakker, G. C. Groenenboom, and G. Meijer, Science **313**, 1617 (2006).
10. E. I. Dashevskaya, I. Litvin, A. I. Maergoiz, E. E. Nikitin, and J. Troe, J. Chem. Phys. **118**, 7313 (2003).
11. E.I Dashevskaya, I. Litvin, E. E. Nikitin, and J. Troe, J.Chem.Phys. **120**, 9989 (2004).
12. E. I. Dashevskaya, I. Litvin, E. E. Nikitin, I. Oref, and J. Troe, J.Phys.Chem. A, **108**, 8703 (2004).
13. E. E. Nikitin, and J. Troe, Phys.Chem.Chem.Phys. **7**, 1 (2005)
14 E. I. Dashevskaya, I. Litvin, E. E. Nikitin, and J. Troe, J.Chem.Phys. **122**, 184311 (2005)
15. A. G. Wickham, T. S. Stoecklin, and D. C. Clary, J. Chem. Phys. **96**, 1053 (1992).

16. J. Troe, Ber. Bunsen-Ges. Phys. Chem. **99**, 341 (1995).
17. E. I. Dashevskaya, I. Litvin, E. E. Nikitin, and J. Troe, Phys. Chem. Chem. Phys. **9**, 1559 (2007).
18. M. Auzinsh, E. I. Dashevskaya, I. Litvin, E. E. Nikitin, and J. Troe, J. Chem. Phys. **128**, 184304 (2008).
19. J. D. Graybeal, *Molecular Spectroscopy* (McGraw-Hill, New York, 1988).
20. D. A. Varshalovich, A. N. Moskalev, and V. K. Khersonskii, *Quantum Theory of Angular Momentum* (World Scientific, Singapore, 1988).
21. M. Mizushima, Phys. Rev. **109,** 1557 (1958).
22. E. Vogt and G. H. Wannier, Phys. Rev. **95**, 1190 (1954).

Captions to Figures

Fig. 1 Qualitative properties of AC potentials (labeled by m) for NO($X^2\Pi_{1/2}, j, \varepsilon$) + ion with j=1/2, 3/2, 5/2 and ε=-1,1 in the range of the interaction energy U/k_B=-0.5 ÷ 0.5K relative to the mean energy of the Λ-doublet. Full lines stand for the accurate and PR potentials when they coincide. When they differ, the latter are represented by dashed lines. The Λ-doubling splitting, which increases linearly with j, is strongly enlarged for clarity. The numbers on top of the figure show the heights of the accurate potential barriers for initially repulsive AC potentials.

Fig. 2. Nonadiabatic transition probabilities $P_{j,m}$ vs. collision energy E for j,m and $j,-m$ AC states (labeled by j,m pairs). The curves are terminated at values of about $P_{j,m}=10^{-3}$, below which $P_{j,m}$ can be calculated analytically. The arrows indicate the Λ-doubling splitting in the free molecule for $j=1/2, 3/2, 5/2$. The hatched inserts give the energy ranges where the capture changes from near-adiabatic to near-sudden.

Fig. 3. Capture of NO($^2\Pi_{1/2,j=1/2,\varepsilon=\pm1}$) by C^+ at $T >> T^{\Lambda}_{1/2}$. Full lines: accurate reduced rate coefficients $\widetilde{\chi}_{1/2,+}$, $\widetilde{\chi}_{1/2,-}$ and $\widetilde{\chi}^{\rm eff}_{1/2}$ (for thermal populations of the Λ-components). The dashed line corresponds to the rate coefficient $\widetilde{\chi}^{\rm AC}_{1/2}$ which is the mean of $\widetilde{\chi}_{1/2,+}$ and $\widetilde{\chi}_{1/2,-}$. The two filled symbols at the l.h.s. correspond to 0.1 K; values for lower T are shown in Figs.6 and 7. A slight decline of the curves at r.h.s. of the figure towards the Langevin limit (marked by the arrow) signals the breakdown of the PR approximation.

Fig. 4. Capture of NO($^2\Pi_{1/2,j=3/2,\varepsilon=\pm1}$) by C^+ at $T >> T^{\Lambda}_{3/2}$. Full lines: accurate reduced rate coefficients, $\widetilde{\chi}_{3/2,+}$, $\widetilde{\chi}_{3/2,-}$, and $\widetilde{\chi}^{\rm eff}_{3/2}$ (for thermal populations of the Λ-components). The dashed line corresponds to the rate coefficient $\widetilde{\chi}^{\rm AC}_{3/2}$ which is the mean of $\widetilde{\chi}_{3/2,+}$ and $\widetilde{\chi}_{3/2,-}$. The shallow minimum for $\widetilde{\chi}_{3/2,+}$, $\widetilde{\chi}^{\rm eff}_{3/2}$ and $\widetilde{\chi}^{\rm sudd}_{3/2}$ results from the interplay of the charge-dipole and charge-quadrupole interaction. The two filled symbols at the l.h.s. of this figure correspond to 0.1 K; values for lower T are shown in Fig 7.

Fig. 5. Capture of NO($^2\Pi_{1/2,j=5/2,\varepsilon=\pm1}$) by C^+ at $T >> T^{\Lambda}_{5/2}$. Full lines: accurate reduced rate coefficients, $\widetilde{\chi}_{5/2,+}$, $\widetilde{\chi}_{5/2,-}$, and $\widetilde{\chi}^{\rm eff}_{5/2}$ (for thermal populations of the Λ-components). The dashed line corresponds to the rate coefficient $\widetilde{\chi}^{\rm AC}_{5/2}$ which is the mean of $\widetilde{\chi}_{5/2,+}$ and $\widetilde{\chi}_{5/2,-}$ The minimum for $\widetilde{\chi}_{5/2,+}$, $\widetilde{\chi}_{5/2,-}$, and $\widetilde{\chi}^{\rm sudd}_{5/2}$ results from the interplay of the charge-quadrupole and weak charge-dipole interaction. The filled symbols at the l.h.s. of this figure correspond to 0.1 K; values for lower T are shown in Fig 7.

Fig. 6. Capture of NO($^2\Pi_{1/2,j=1/2,\varepsilon=+1}$) by C^+ in the region around $T \approx T^{\Lambda}_{1/2}$ (marked by the arrow). The symbols correspond to the accurate PR rate coefficient $\widetilde{\chi}^{\rm PR}_{1/2,+}$, the full line to $\widetilde{\chi}^{\rm PR,eff}_{1/2,+}$ and the dots to $\widetilde{\chi}^{\rm PR,app}_{1/2,+}$. The dashed lines correspond to the extrapolations of $\chi^{\rm PR}_{1/2,+}$ and $\chi^{\rm PR,eff}_{1/2}$ from $T >> T^{\Lambda}_{1/2}$ to lower temperatures. The two filled symbols at the r.h.s. of this figure correspond to those at the l.h.s. of Fig 3. The arrow at the l.h.s. of this figure corresponds to the low-temperature limit of the capture rate coefficients from the lowest HF state ($F = 3/2$) of the lower component of the Λ-doublet, see Section 5.

Fig. 7. Capture of NO($^2\Pi_{1/2,j,\varepsilon=\pm1}$) by C^+ in the region around $T \approx T_j^{\Lambda}$ (marked by the arrows) for $j = 1/2, 3/2, 5/2$. The open symbols correspond to the reduced rate coefficients $\widetilde{\chi}_{j,\varepsilon}^{\mathrm{PR}}$, and the full lines represent $\widetilde{\chi}_{j,\varepsilon}^{\mathrm{PR,eff}}$. The filled symbols at the r.h.s. of this figure correspond to those at the l.h.s. of Figs 3–5.

Fig. 8. Scaled adiabatic channel potentials for NO($^2\Pi_{1/2,j=1/2,\,\varepsilon=\pm1,\,F=1/2,\,3/2}$) + ion system (relative to the Λ-doubling spacing without HF interaction) vs. scaled cd interaction energies between free molecular states ($\eta = 0$) and medium-values of the cd interaction ($\eta = 6$). The full lines correspond to accurate potentials with $M = \pm 1/2$ (unmarked) and with $M = \pm 3/2$ (marked). The dashed lines correspond to second-order Stark effect with respect to HF where F and ε are good quantum numbers. The dotted lines correspond to an intermediate Stark effect without HF interaction.

Fig. 9. Scaled adiabatic channel potentials for the NO($^2\Pi_{1/2,j=1/2,\varepsilon}$) + ion system vs. cd interaction energy from medium-values of the cd interaction ($\eta = 4$) to very large cd interaction ($\eta = 60$) (scaled as in Fig.8). The full lines correspond to accurate potentials (unmarked and marked for $M = \pm 1/2$ and $M = \pm 3/2$ respectively), the dotted lines to first-order Stark effect with respect to Λ-doubling states where m and $\widetilde{\Omega}$ become good quantum numbers. This figure overlaps with Fig. 8 over the range $4 < \eta < 6$.

Table 1. Relevant parameters of the NO($X^2\Pi_{1/2}$) molecule

	B_{eff}	D_{e}	ρ	$K_{1/2}$	d
MHz	50124	0.016	355.2	46.3	112.6
C m^{-1}	1.67	$5.33 \cdot 10^{-7}$	0.0118	$1.54 \cdot 10^{-3}$	$3.75 \cdot 10^{-3}$
Kelvin	2.41	$7.68 \cdot 10^{-7}$	0.0170	$2.22 \cdot 10^{-3}$	$5.40 \cdot 10^{-3}$

$\mu_{\text{D}} = 0.063\,\text{au} = 0.16\,\text{D} = 1.60 \cdot 10^{-19}\ \text{esu} \cdot \text{cm}$; $\alpha = 1.680 \cdot 10^{-24}\ \text{cm}^3 = 11.337\ \text{a.u.}$;

$Q = -2.421 \cdot 10^{-26}\ \text{esu} \cdot \text{cm}^2 = 1.80\ \text{a.u.}$

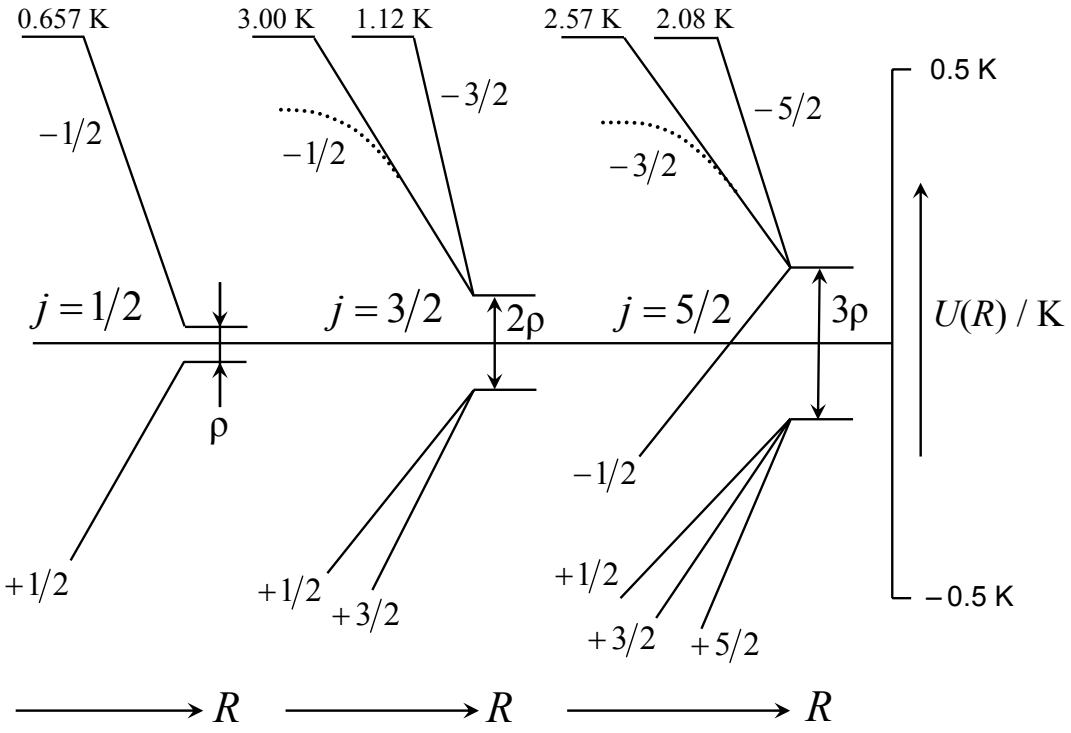
0.657 K
3.00 K
1.12 K
2.57 K
2.08 K
0.5 K
−1/2
−3/2
−1/2
−5/2
−3/2
j = 1/2
j = 3/2
2ρ
j = 5/2
3ρ
U(R) / K
ρ
−1/2
+1/2
+1/2
+3/2
+1/2
+3/2
+5/2
−0.5 K
R
R
R

Figure 1

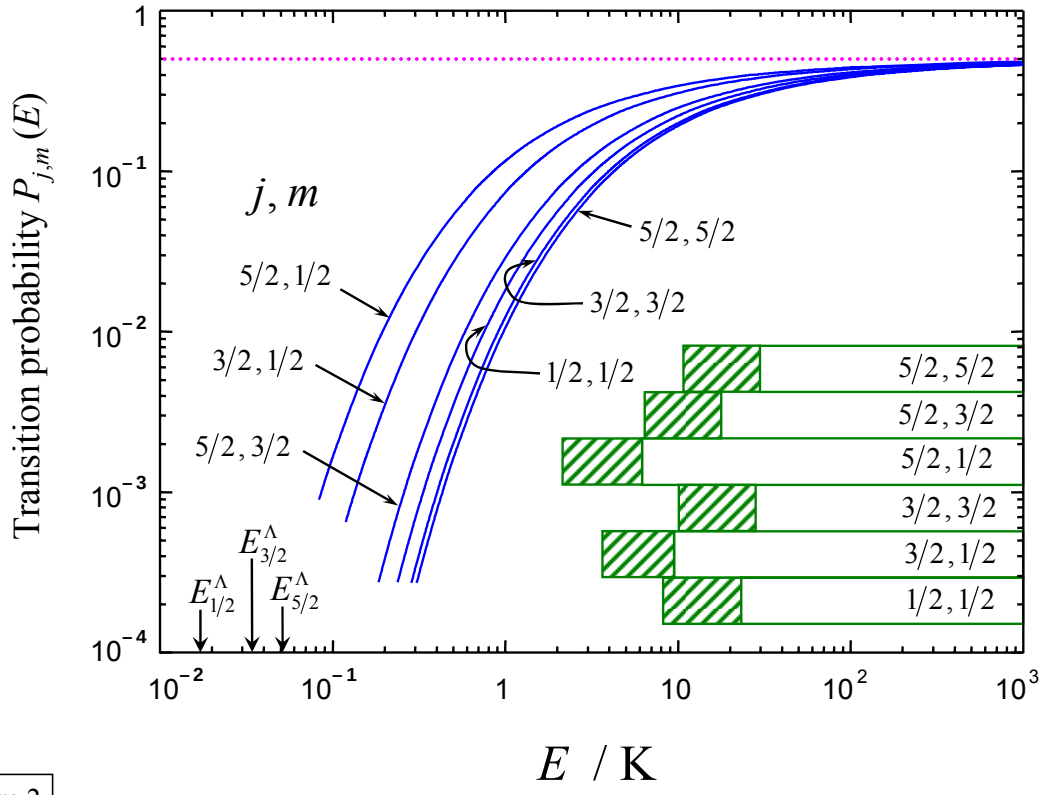
Transition probability $P_{j,m}(E)$
E / K
j, m
5/2, 1/2
3/2, 1/2
5/2, 3/2
5/2, 5/2
3/2, 3/2
1/2, 1/2
$E^{\Lambda}_{1/2}$
$E^{\Lambda}_{3/2}$
$E^{\Lambda}_{5/2}$
5/2, 5/2
5/2, 3/2
5/2, 1/2
3/2, 3/2
3/2, 1/2
1/2, 1/2

Figure 2

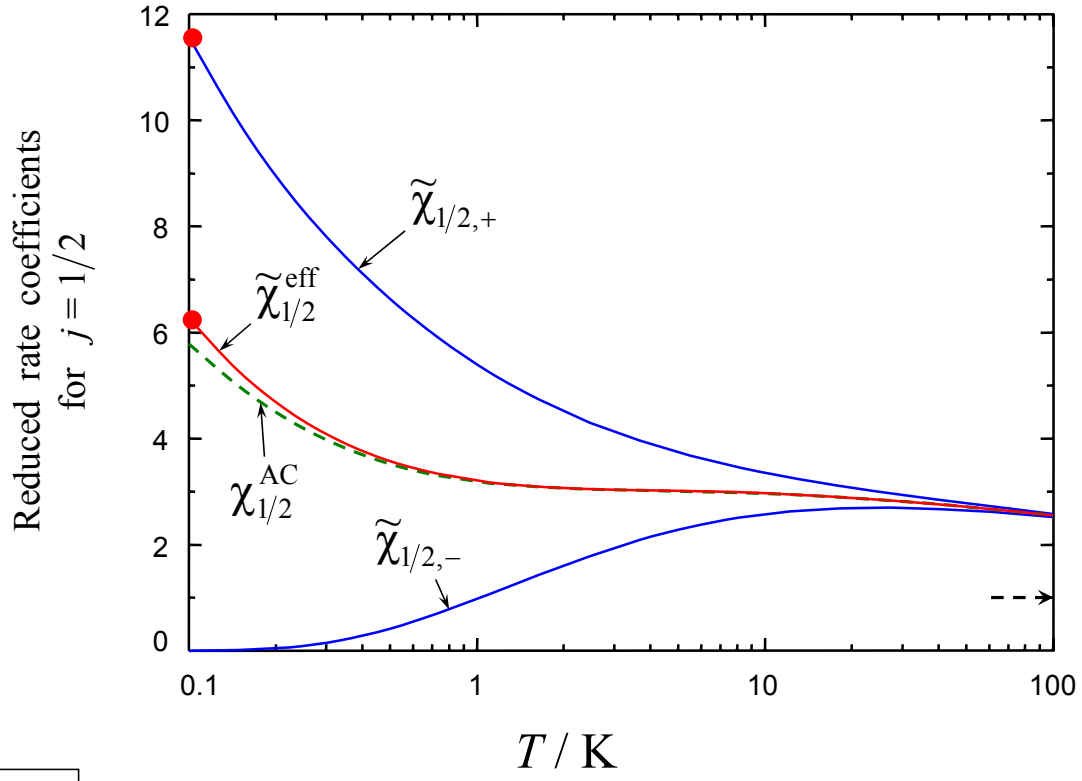
Reduced rate coefficients for $j = 1/2$
12
10
8
6
4
2
0
0.1
1
10
100
T / K
$\tilde{\chi}_{1/2,+}$
$\tilde{\chi}^{\mathrm{eff}}_{1/2}$
$\chi^{\mathrm{AC}}_{1/2}$
$\tilde{\chi}_{1/2,-}$

Figure 3

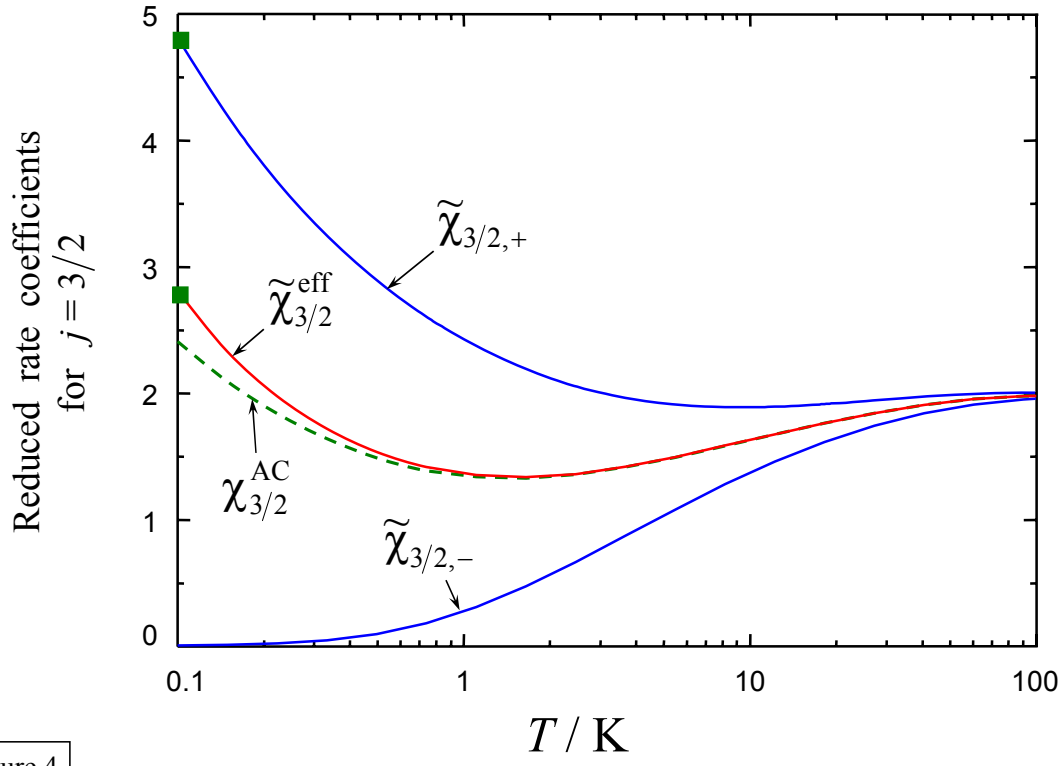
Reduced rate coefficients
for $j = 3/2$
5
4
3
2
1
0
0.1
1
10
100
T / K
$\tilde{\chi}_{3/2,+}$
$\tilde{\chi}^{\mathrm{eff}}_{3/2}$
$\chi^{\mathrm{AC}}_{3/2}$
$\tilde{\chi}_{3/2,-}$

Figure 4

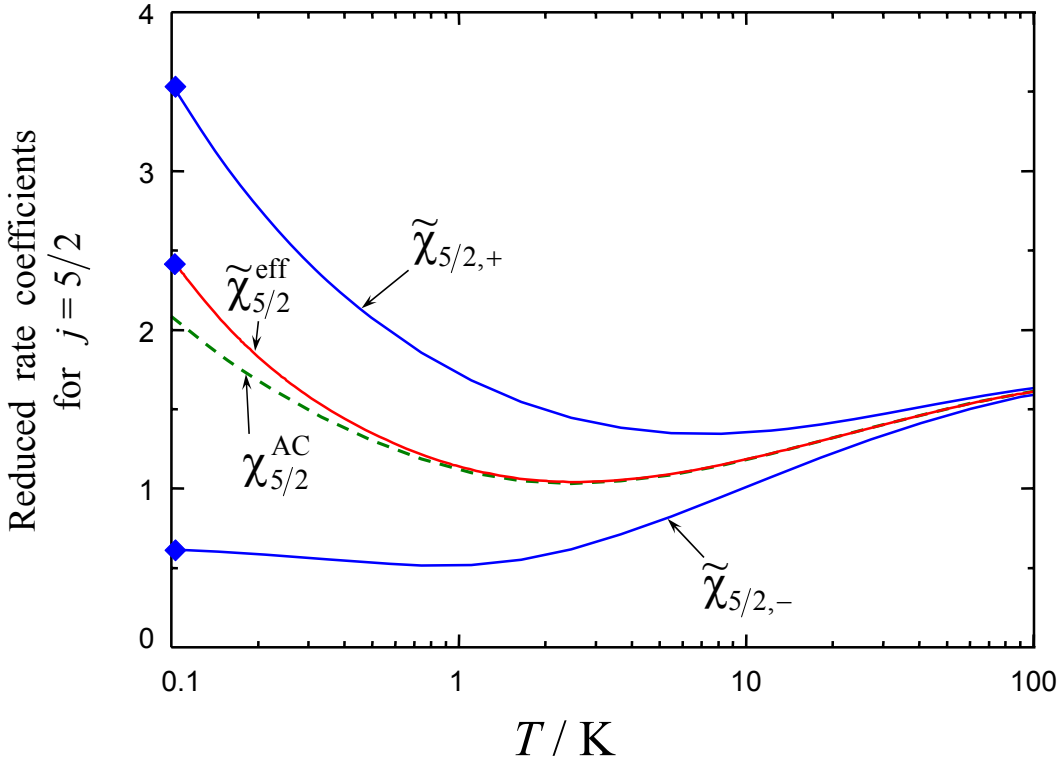
Reduced rate coefficients for $j = 5/2$
$\tilde{\chi}_{5/2,+}$
$\tilde{\chi}^{\mathrm{eff}}_{5/2}$
$\chi^{\mathrm{AC}}_{5/2}$
$\tilde{\chi}_{5/2,-}$
T / K
0
1
2
3
4
0.1
1
10
100

Figure 5

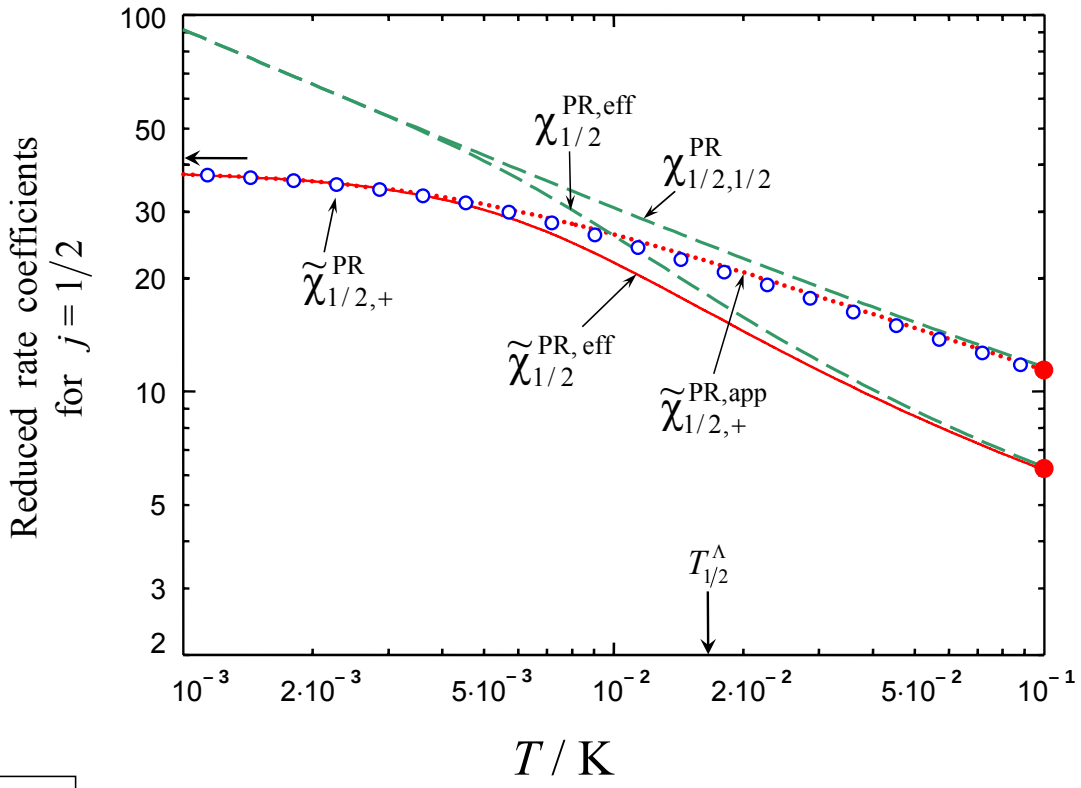
Reduced rate coefficients for $j = 1/2$
100
50
30
20
10
5
3
2
$\chi^{\mathrm{PR,eff}}_{1/2}$
$\chi^{\mathrm{PR}}_{1/2,1/2}$
$\tilde{\chi}^{\mathrm{PR}}_{1/2,+}$
$\tilde{\chi}^{\mathrm{PR,\,eff}}_{1/2}$
$\tilde{\chi}^{\mathrm{PR,app}}_{1/2,+}$
$T^{\Lambda}_{1/2}$
10^{-3}
$2{\cdot}10^{-3}$
$5{\cdot}10^{-3}$
10^{-2}
$2{\cdot}10^{-2}$
$5{\cdot}10^{-2}$
10^{-1}
T / K

Figure 6

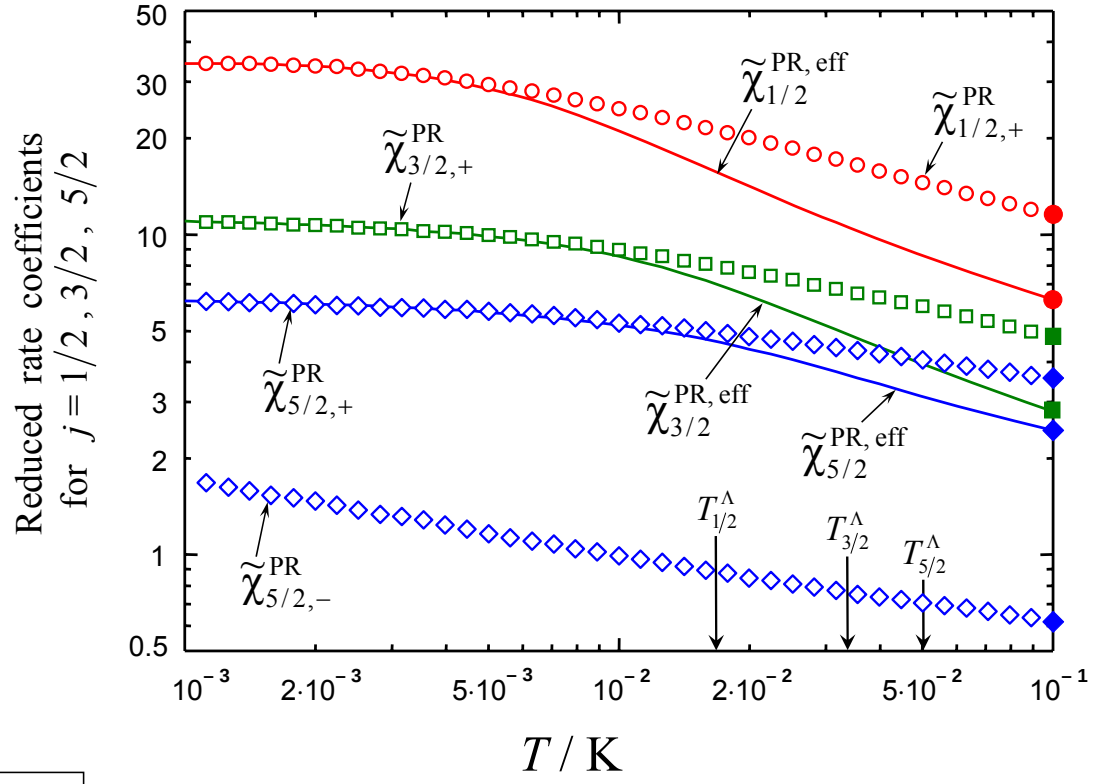
Reduced rate coefficients
for $j = 1/2, 3/2, 5/2$
50
30
20
10
5
3
2
1
0.5
10^{-3}
$2{\cdot}10^{-3}$
$5{\cdot}10^{-3}$
10^{-2}
$2{\cdot}10^{-2}$
$5{\cdot}10^{-2}$
10^{-1}
T / K
$\tilde{\chi}^{\mathrm{PR,\,eff}}_{1/2}$
$\tilde{\chi}^{\mathrm{PR}}_{1/2,+}$
$\tilde{\chi}^{\mathrm{PR}}_{3/2,+}$
$\tilde{\chi}^{\mathrm{PR}}_{5/2,+}$
$\tilde{\chi}^{\mathrm{PR,\,eff}}_{3/2}$
$\tilde{\chi}^{\mathrm{PR,\,eff}}_{5/2}$
$\tilde{\chi}^{\mathrm{PR}}_{5/2,-}$
$T^{\Lambda}_{1/2}$
$T^{\Lambda}_{3/2}$
$T^{\Lambda}_{5/2}$

Figure 7

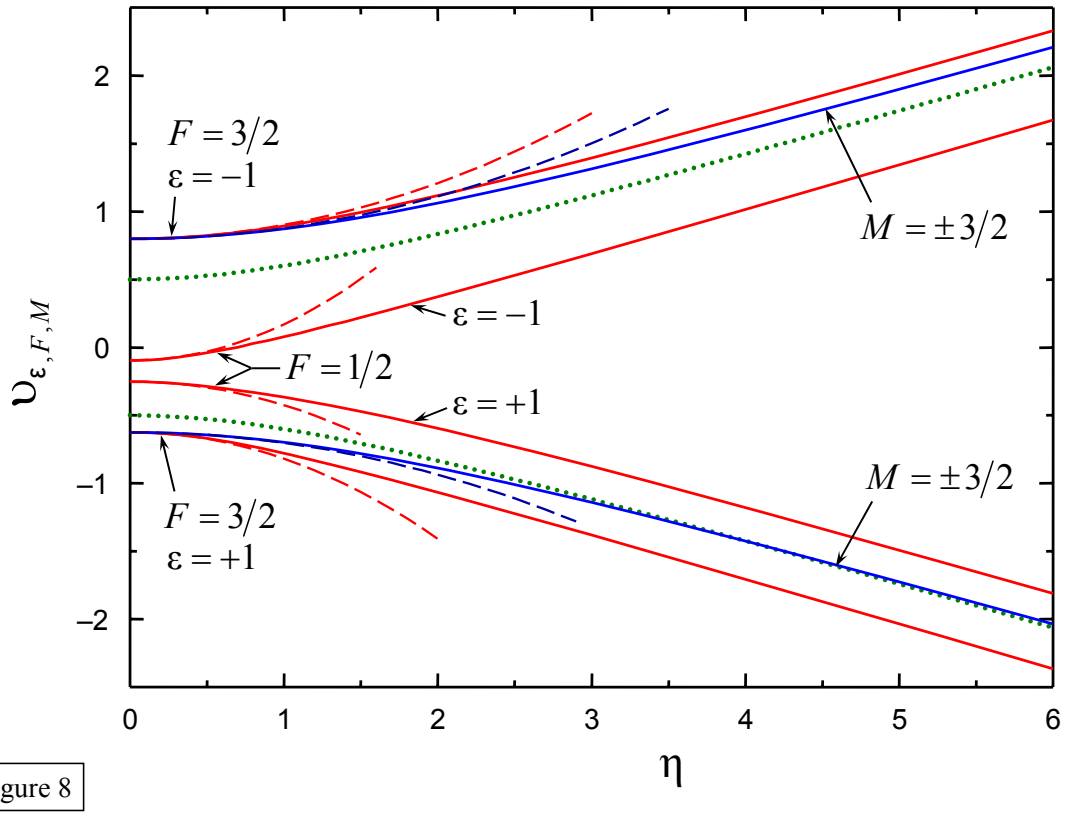
$F = 3/2$
$\varepsilon = -1$
$M = \pm 3/2$
$\varepsilon = -1$
$F = 1/2$
$\varepsilon = +1$
$M = \pm 3/2$
$F = 3/2$
$\varepsilon = +1$
$\upsilon_{\varepsilon,F,M}$
η
2
1
0
−1
−2
0
1
2
3
4
5
6

Figure 8

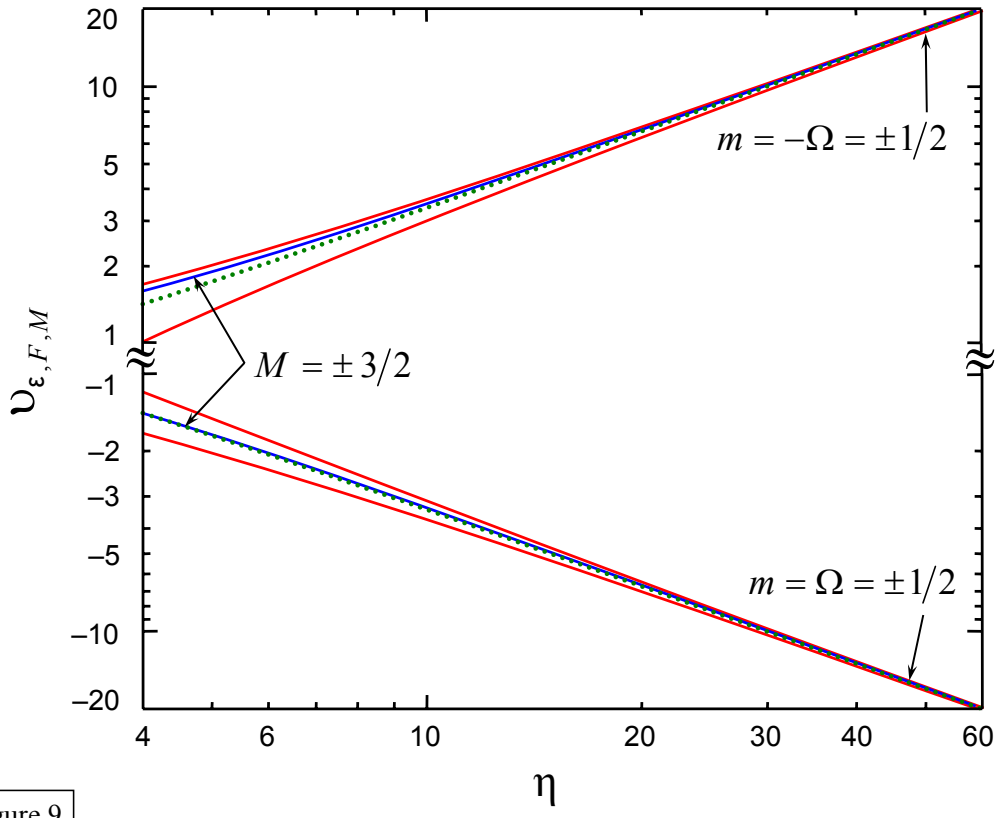
20
10
5
3
2
1
−1
−2
−3
−5
−10
−20
4
6
10
20
30
40
60
η
$\upsilon_{\varepsilon,F,M}$
$m = -\Omega = \pm 1/2$
$M = \pm 3/2$
$m = \Omega = \pm 1/2$

Figure 9